PAPER • OPEN ACCESS

Functionalizing Fe adatoms on Cu(001) as a nanoelectromechanical system

To cite this article: Michael Schüler *et al* 2017 *New J. Phys.* **19** 073016

New Journal of Physics
The open access journal at the forefront of physics

Deutsche Physikalische Gesellschaft DPG
IOP Institute of Physics

Published in partnership with: Deutsche Physikalische Gesellschaft and the Institute of Physics

OPEN ACCESS

RECEIVED
16 December 2016

REVISED
21 May 2017

ACCEPTED FOR PUBLICATION
12 June 2017

PUBLISHED
12 July 2017

PAPER

Functionalizing Fe adatoms on Cu(001) as a nanoelectromechanical system

Michael Schüler[1], **Levan Chotorlishvili**[1], **Marius Melz**[1], **Alexander Saletsky**[2], **Andrey Klavsyuk**[2], **Zaza Toklikishvili**[3] **and Jamal Berakdar**[1]

[1] Institut für Physik, Martin-Luther-Universität Halle-Wittenberg, D-06099 Halle, Germany
[2] Faculty of Physics, Moscow State University, Moscow 119991, Russia
[3] Department of Physics, Tbilisi State University, Chavchavadze Avenue 3, 0128 Tbilisi, Georgia

E-mail: jamal.berakdar@physik.uni-halle.de

Keywords: nanomechanics, nanomagnetism, solid-state based quantum information, spin dynamics, spin–phonon coupling

Abstract

This study demonstrates how the spin quantum dynamics of a single Fe atom adsorbed on Cu(001) can be controlled and manipulated by the vibrations of a nearby copper tip attached to a nano cantilever by virtue of the dynamic magnetic anisotropy. The magnetic properties of the composite system are obtained from *ab initio* calculations in completely relaxed geometries and turned out to be dependent considerably on the tip-iron distance that changes as the vibrations set in. The level populations, the spin dynamics interrelation with the driving frequency, as well as quantum information related quantities are exposed and analyzed.

1. Introduction

Microelectromechanical or nanoelectromechanical systems (NEMS) are at the verge of the classical–quantum world [1–4] and can thus sense, possibly coupled, quantum–classical properties. For instance, tiny vibrating cantilever were shown to detect a single spin [5]. The sensitivity depends on the mean phonon number with the cantilever dynamics turning quantum as the phonons number decreases. Related to these observations, this field promises a new rout to quantum information nanomechanical devices. An example is the setup consisting of a single nitrogen-vacancy (NV) center in a diamond nanocrystal deposited at the extremity of a SiC nanowire [6]. The quantum NV spin dynamics is observed to be coupled to the nanomechanical oscillator by means of the time-resolved nanocrystal fluorescence and photon-correlation measurements. This dynamic can be influenced by external fields such as a non-homogeneous magnetic field. A clear advantage of utilizing the spin-degrees of freedom of the NV is their long decoherence times even at room temperatures [7–12]. Further phenomena emerge when considering strongly coupled nonlinear NEMS in which case phenomena such as nonlinear resonances can be exploited for the control of the energy transfer between the coupled NEMS [13–16].

In the present work we propose a new type of NEMS based on a single magnetic Fe adatom deposited on a Cu(001) substrate. A proper choice of the driving frequency allows controlling the level populations in the system. The proposed (scanning-tunneling microscopy) STM-type or (atomic force microscopy) AFM-type setup is thus a hybrid system utilizing the quantum nature of single adsorbed atoms or molecules on the surface, which were designed as studied in an impressively controllable way experimentally (for example in [17–19]). The magnetic properties of Fe and Co adatoms on a $Cu_2N/Cu(100)$-c (2×2) surface were determined experimentally via x-ray magnetic dichroism measurements [20].

The possibly classical cantilever dissipative dynamics is coupled the quantum spin dynamics of the adsorbates since, as demonstrated below, the magnetic anisotropy is affected by the tip-adsorbate distance, and hence by the tip vibrational motion. This coupling might be exploited to access the topology or the local magnetic properties of spin systems [21].

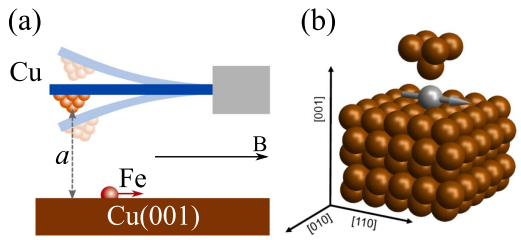

Figure 1. (a) The prototypical model system for coupling the spin dynamics of a single magnetic Fe adatom on the Cu(001) substrate to the mechanical vibrations of a nano-sized cantilever. (b) The cluster used to represent the copper substrate, the copper tip and the Fe adatom.

2. Theoretical framework

Specifically, we consider a single magnetic Fe atom deposited on a Cu(001) surface. A similar setup consisting of Fe or Mn on copper coated by an Cu_2N overlayer, was shown to have a large magnetic anisotropy and relaxation times [17, 22]. Our calculations are carried out in the presence of a tip apex as in AFM experiments and reveal a substantial dependence of the magnetic anisotropy on the distance between the tip and the Fe adatom. Thus, in the proposed setup the magnetic properties of the single-atom are coupled to the oscillations of a nano-sized cantilever carrying the tip apex (figure 1(a)). As the characteristic frequencies of such nano-mechanical oscillators are known to reach the gigahertz regime [23], frequencies in the range of ∼100 GHz become feasible upon a further downscaling of the cantilever and can thus match the typical energy scale of the spin system (which is in the range of few meV).

3. *ab initio* calculations

Ab initio density-functional calculations of the ground state and the energy difference upon changing the magnetization axis of the Fe atom were performed using the projector augmented-wave technique [24, 25], as implemented in the Vienna *ab initio* simulation package [26]. The calculations are based on density-functional theory with the generalized gradient approximation [27, 28]. We used the same methodology used in previous calculations of the magnetic anisotropy of Co and Fe adatoms on Rh(111), Pt(111) and Cu(100) substrates [29–31]. We note in this context that STM experiments were performed after the tip were in contact with the surface, and hence the tip is most likely covered by the surface material [32]. In this case a tip with surface atoms is often used in computer calculations [33, 34].

Our computational models consists 125 copper atoms representing the surface, the iron atom, and five additional atoms for simulating the presence of a tip apex, as depicted in figure 1(b). The unit cell has a size of 12.87 Å in the x and y directions (parallel to the surface), whereas the extent of the z direction (perpendicular to the surface) amounts to 31.89 Å. At this slab thickness, the interaction between the tip and the repeated image of the surface is negligible. A cutoff energy of 300 eV is used. The calculations including spin–orbit coupling require a fine k-point mesh for the Brillouin-zone integrations. Test calculations were performed for iron atom on a Cu(001) surface for three different k-point grids: $3 \times 3 \times 1$, $3 \times 3 \times 2$, and $5 \times 5 \times 1$ generated by the Monkhorst–Pack scheme [35], in conjunction with a modest Gaussian smearing method. A $3 \times 3 \times 1$ grid provided the best compromise between accuracy and computational efforts.

The calculations were performed in two steps. First the coordinates of the iron atom and the positions of the atoms in the three topmost layers of the substrate (apart from the tip) were optimized using scalar-relativistic calculations until the forces on all unconstrained atoms were converged to less than 0.01 eV $Å^{-1}$. In the second step, the geometry and the electronic and magnetic ground states resulting from the scalar-relativistic calculations were used to initialize the relativistic calculations including spin–orbital coupling. Recent work [36] demonstrated that relaxations of Fe and Co adatom on Pt(111) with and without spin–orbit coupling are almost identical.

After a geometry optimization of the full cluster (apart from the tip) for every position of the tip, we computed the magnetic anisotropy energy as the difference of the respective ground state energies upon varying the magnetization axis. We found that the dependence on the angle θ measured from the Fe-tip axis is well described by the lowest-order anisotropy term $\delta \sin^2 \theta$, as it is known for similar systems. The dependence on the angle ϕ measured along the plane on the other hand turned out to be rather weak. Furthermore, we analyzed the spin density $n_\uparrow(\mathbf{r}) - n_\downarrow(\mathbf{r})$ to investigate the degree of localization of the magnetization. The result is presented in figure 2 for small values of the density in two characteristic planes along the symmetry directions. We

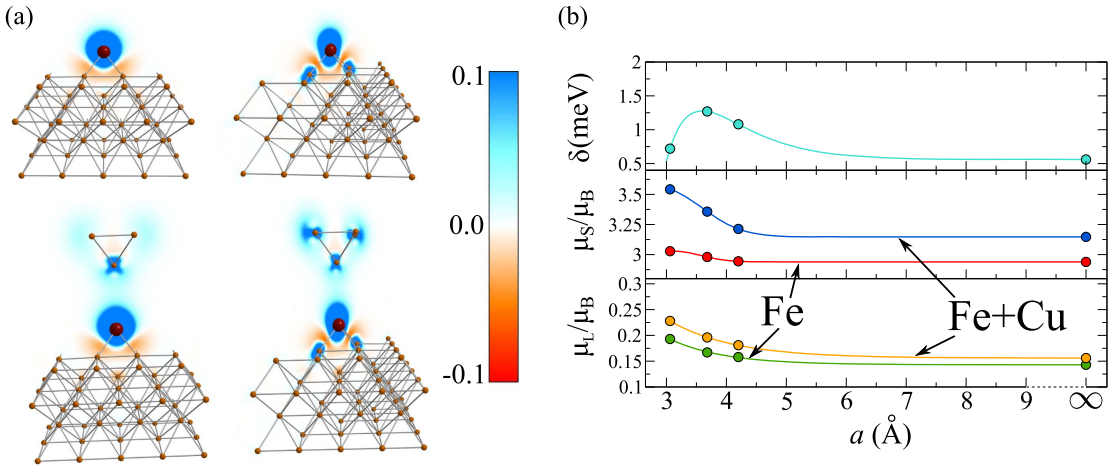

Figure 2. (a) The spin density of Cu–Fe system without tip (upper two figures), and with the tip situated 4.5 Å above the adsorbate (lower two figures). We show cuts of the spin density (unit: $Å^{-3}$) along the planes passing through the Fe atom (0, 1, 0) (upper and lower left) and (1, 1, 0) (upper and lower right figures). The number of atoms shown were reduced to emphasize the C_{4v} symmetry. (b) The prefactor of the anisotropy (upper panel), the magnetic moment originating from the spin (middle panel), and from the orbital moment (lower panel). A positive sign of the magnetic anisotropy parameter corresponds to a perpendicular easy axis. The values from our *ab initio* calculations (dots) are well described by Gaussian-type fitting functions (full lines). The red and the green curves correspond to the values when integrating the spin density over a small sphere around the Fe atom, whereas the neighboring Cu atoms have been also included for the blue and the orange curves.

conclude that the Fe atom slightly polarizes the tip and the substrate below. Especially for the latter we observe the typical behavior of a spin density associated with this kind of anisotropy.

However, the major contribution to the magnetization is confined within the direct vicinity of the Fe atom, confirming that the effective surface spin can be interpreted as the magnetic moment of few atoms.

4. Modeling the spin dynamics

In figure 2(b) we show our results for the dependence of the magnetic anisotropy parameter δ and of the magnetic moments associated with the spin (μ_S), and the angular momentum (μ_L) for four different values of the distance a between the last tip atom and the iron atom. The spin magnetic moment on the iron atom without the tip-adatom interaction is 2.94 μ_B. This result agrees well with previous density functional calculations [37]. It should be noted, that the magnetic anisotropy parameter δ for an atom on the surface is very sensitive to the interatomic distances [38, 39] and the arrangement of the atom [29, 40]. It was demonstrated that the structural relaxation of the adatom and the substrate reduces significantly the magnetic anisotropy energy [38, 39]. Therefore, compared to *ab initio* calculations for the Fe adatom on the ideal Cu(001) surface, our magnetic anisotropy energy obtained in a fully relaxed geometry is several times less than the value presented in [41].

Based on the fitting functions displayed in figure 2(b) we are now able to formulate the Hamiltonian describing the effective surface angular momentum with the parametric dependence on a as

$$\hat{H}(a) = -[g_S(a) + g_L(a)]\mu_B B_0 \hat{J}_x - \delta(a)\hat{J}_z^2. \quad (1)$$

We assume a magnetic field with a strength B_0 is applied along the x axis. Approximating the total angular momentum with 2 turns out to be an adequate description and can be confirmed experimentally by means of inelastic tunneling spectroscopy [17, 22]. The distance-dependent gyromagnetic ratios for spin (angular) momentum $g_S(a)$ ($g_L(a)$) account for the varying magnitude of the total magnetic moment (see figure 2(b)), as extracted from our *ab initio* calculations. We fix B_0 to the value of 4 T and take the ground state as the initial state. As one can readily show for equation (1), the expectation value with respect to all eigenstates of $\hat{J}_y$ and $\hat{J}_z$ is exactly zero. This holds true even for the case of the time-dependent Schrödinger equation, when replacing $a \rightarrow a(t)$.

To map out the spin dynamics for a representative case we choose a by $a_0 = 4$ Å and $B_0 = 4$ T. The energies of the eigenstates $|\xi_n\rangle$ (on the ordinate axis) and the expectation values of J_x (abscissa) are shown in the inset in figure 3. For a high density of phonons the spin dynamics originates from an oscillation of the tip apex according to $a(t) = a_0 + b\sin(\omega t)$ for $t > 0$ (we assume $a(t) = a_0$ for $t \leqslant 0$). This corresponds to a setup where the system is initially in its ground state and is driven out of equilibrium by the cantilever oscillations for $t > 0$. The oscillation amplitude is chosen as $b = 0.9$ Å.

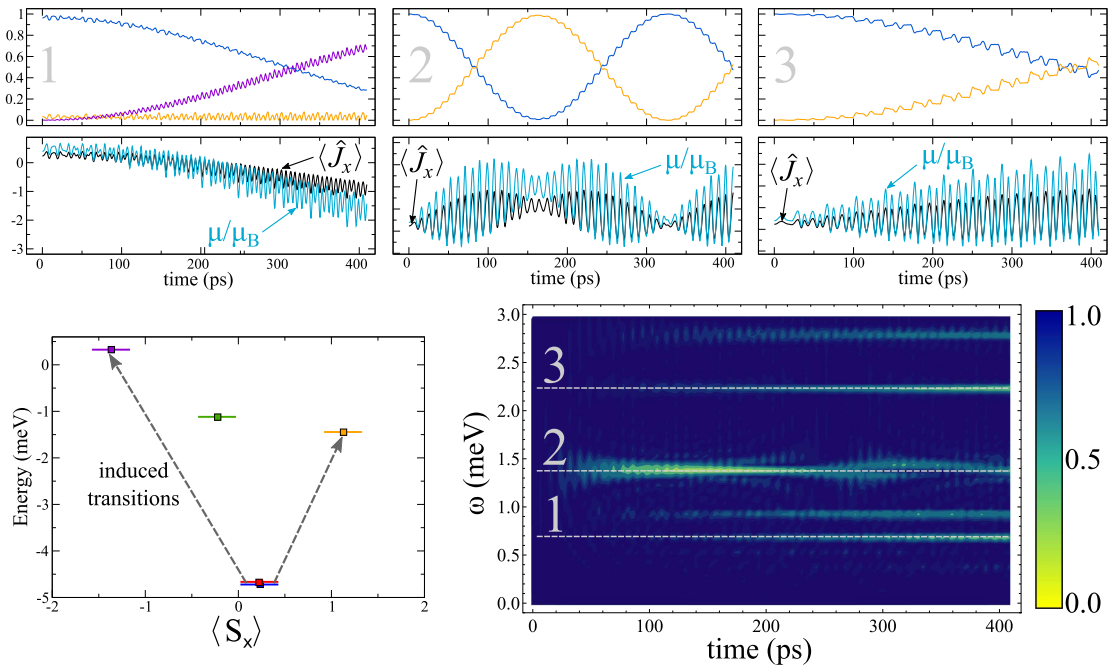

Figure 3. The population dynamics arising due to the periodic driving $a(t)$. The lower panels show the initial configuration (left), and the probability to measure the ground state as a function of the time and the driving frequency ω (right). The gray dashed lines with their respective labels 1, 2 and 3 denote three selected frequencies. The corresponding population and the spin dynamics are displayed in the upper three panels.

Before discussing the results, let us elaborate on the qualitative aspects of the dynamics. Since the spin is driven by an effectively time-dependent anisotropy, i.e., the coupling to the operator $\hat{J}_z^2$, the induced transitions allow for changing the spin projection $\langle \hat{J}_x \rangle$ only. The magnetic moment μ will thus remain parallel to $\langle \hat{J}_x \rangle$. Therefore, only the longitudinal spin dynamics can be induced, limiting the transitions from the ground state to only the two excited states that match in symmetry.

In figure 3 we present the resulting spin dynamics in dependence on ω. The color map plot (lower right figure) shows the population of the ground state (which we have chosen as the initial state). Interestingly, the magnetic moment is hardly affected by the variation of the magnetic anisotropy for the major part of the frequency range. Apart from that, a couple of distinct lines indicate an optimal setting for the parameters to drive the angular momentum to some excited states. A more detailed analysis reveals that the dynamics for the frequencies indicated by the dashed lines (labeled by 1, 2, 3) exhibits almost Rabi-like transitions from the ground state to a single excited state. This behavior can be explored further by a Floquet analysis. We therefore expand the angular momentum wave function as

$$|\xi(t)\rangle = \sum_{n=1}^{2J+1} c_n |\phi_n(t)\rangle = \sum_{n=1}^{2J+1} c_n e^{i\varepsilon_n t} |f_n(t)\rangle, \tag{2}$$

where ε_n are the quasi energies and $|\phi_n(t)\rangle = e^{i\varepsilon_n t}|f_n(t)\rangle$ the Floquet eigenvectors. Both can be obtained by solving the eigenvalue problem of the time-evolution operator $U(t, 0)$ at $t = T \equiv 2\pi/\omega$, since

$$\hat{U}(T, 0)|f_n(0)\rangle = e^{i\varepsilon_n T}|f_n(0)\rangle \tag{3}$$

(note that $|f_n(t + T)\rangle = |f_n(t)\rangle$). Before discussing the solution of equation (3), let us briefly revisit how the dynamics shown in figure 3 can be explained within the Floquet theory. Equation (2) expresses the expansion of the time-dependent spin state in terms of the orthonormal Floquet states $|f_n(t)\rangle$, with the projection coefficients c_n. For the case $c_n = c_{n_0}\delta_{n,n_0}$, the projection $\langle \xi(0)|\xi(t)\rangle$ amounts to $\exp[-i\varepsilon_{n_0} t]\langle f_{n_0}(0)|f_{n_0}(t)\rangle$, such that the population of the initial state remains one at multiples of T. Assuming on the other hand $c_n = (\delta_{n,n_1} \pm \delta_{n,n_2})/\sqrt{2}$ yields the stroboscopic time evolution

$$|\langle \xi(0)|\xi(kT)\rangle|^2 = \cos^2[(\varepsilon_{n_1} - \varepsilon_{n_2})kT]. \tag{4}$$

These two scenarios explain the dynamics observed in figure 3, where slow, Rabi-like population transfer (with a frequency corresponding to the difference of two quasienergies) is overlayed with fast oscillations (which originate from the overlaps of the type $\langle f_n(0)|f_m(t)\rangle$ and are thus periodic with the frequency ω). The quasienergies obtained from equation (3) are presented in figure 4(a) (upper panel), along with the projection $|c_n|^2 = |\langle \xi(0)|f_n(0)\rangle|^2$ (lower panel). As pointed out, the decisive factor for the depletion of the ground state is at

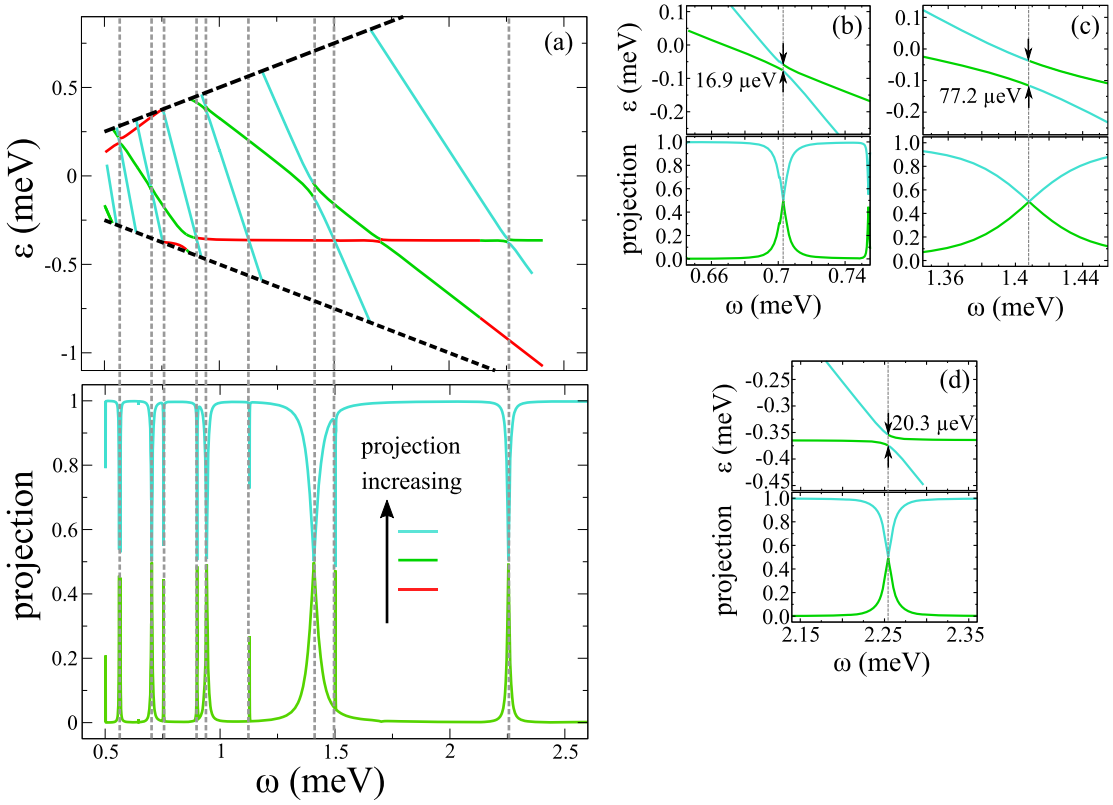

Figure 4. (a) Upper panel: the quasienergies ε_n (folded back to the first Brioullin zone, indicated by the black dashed line) as a function of the driving frequency ω. The color coding corresponds to the projection of the eigenvectors $|f_n(0)\rangle$ onto the initial state, $|\langle\xi(0)|f_n(0)\rangle|^2$, which is displayed in the lower panel. The vertical gray lines connect the points where the projection approaches 1/2 with the avoided crossing points. (b) A zoom around $\omega = 0.704$ meV , (c) $\omega = 1.408$ meV and (d) $\omega = 2.254$ meV. The gap width of the crossings is given in the inset.

least two projection coefficients being different from zero. For this reason, we have ordered the quasienergies according to the magnitude of $|c_n|^2$. As it turned out, only two of the Floquet states display a significant contribution to the initial state. Therefore, only their projection is shown in figure 4(a). For the complete picture of the behavior of the quasienergies however, the third state and its eigenvalue are included in the upper panel.

The vertical lines in figure 4(a) demonstrate that the scenario for the dynamics according to equation (4) occurs only at the crossing points of the quasienergies, where (at least) two branches exchange their character, that is the magnitude of their projection coefficients. A more detailed analysis reveals that all crossings are avoided crossings. The difference of the quasienergies becomes thus relatively small, leading to the slow dynamics in figure 3. For the exemplary values of ω, figures 4(b) and (c) provides a magnification of the crossing points and gives their width. Converting the quasienergy gap into a time scale results in exactly the characteristic time of the slow dynamics in figure 3.

5. Entanglement measures

With cooling down the system, oscillations of the nanocantilever become inherently quantum. Thus the nanocantilever can detect inter-level transitions of the single spin. This statement is generic for a broad class of the nanomechanical systems and is valid for our model as well. Our model is exactly solvable (which is in fact its merit) and allow to explore analytically the entanglement between the cantilever and the system. In contrast to the above, where we investigated the case of a moderate elongations of the cantilever, leading to a nonlinear coupling, we consider linear coupling only. In addition to the feasibility of analytical solutions, the quantum fluctuations and the oscillations of the cantilever occur on a smaller scale, while large elongations are associated with the classical case which is studied above.

In order to quantify the entanglement in the system, we explore von Neumann entropy. In the quantum information theory the von Neumann entropy is known as the 'entanglement entropy' of the reduced density matrix. The technical details of the von Neumann entropy and hence of the reduced density matrix in our case are given in the appendix.

To construct a quantized model, the tip-substrate distance is replaced by $a \rightarrow a_0 + \Delta a \sum_\alpha (\hat{a}_\alpha + \hat{a}_\alpha^\dagger)$, where $\hat{a}_\alpha^\dagger$ ($\hat{a}_\alpha$) is the creation (annihilation) operator of the cantilever modes. Modern technologies enabled the fabrication of dual mode ($\alpha = 1, 2$) cantilevers, for more details see [42, 43].

The resulting Hamiltonian, in lowest order in the oscillation amplitude Δa reads

$$\hat{H} = -[g_S(a_0) + g_L(a_0)]\mu_B B_0 \hat{J}_x + \sum_\alpha \Omega_\alpha \hat{a}_\alpha^\dagger \hat{a}_\alpha - \Delta a \delta'(a_0) \hat{J}_z^2 \sum_{\alpha=1,2} (\hat{a}_\alpha + \hat{a}_\alpha^\dagger). \tag{5}$$

Similar to the classical case analyzed above, the transition operator $\hat{J}_z^2$ allows the transition from the ground state to two excited states only. Hence, the Hamiltonian (5) can be reduced to a three-level system in spin space. We assume that the cantilever frequencies $\Omega_{1,2}$ match the excitation energies $\omega_{1,2} = E_{1,2} - E_0$.

We solve directly analytically for the Schrödinger equation

$$\mathrm{i}\frac{\partial|\Psi\rangle}{\partial t} = \hat{H}|\Psi\rangle, \tag{6}$$

using the following ansatz

$$\begin{aligned}|\Psi(t)\rangle = {} & C_1(t)|n_1, n_2, 1\rangle + C_2(t)|n_1 - 1, n_2, 2\rangle + C_3(t)|n_1, n_2 - 1, 3\rangle \\ & + C_4(t)|n_1, n_2, 4\rangle + C_5(t)|n_1, n_2, 5\rangle.\end{aligned} \tag{7}$$

Here n_1, n_2 quantify the number of phonons in the cavity with the frequencies Ω_1, Ω_2. Taking into account equations (6) and (7) we consider the resonance condition $E_2 - E_1 \approx \Omega_1$, $E_3 - E_1 \approx \Omega_2$. After standard calculations we obtain

$$\begin{aligned}C_1(t) = {} & \exp(-\mathrm{i}\Delta_1 t)\{C_1(0)\cos(\gamma\sqrt{n_1 + n_2}\, t) \\ & - \mathrm{i}\frac{C_2(0)\sqrt{n_1}\sin(\gamma\sqrt{n_1 + n_2}\, t)}{\sqrt{n_1 + n_2}} \\ & - \mathrm{i}\frac{C_3(0)\sqrt{n_2}\sin(\gamma\sqrt{n_1 + n_2}\, t)}{\sqrt{n_1 + n_2}}\Bigg\},\end{aligned} \tag{8}$$

$$\begin{aligned}C_2(t) = {} & \exp(-\mathrm{i}(\Delta_2 - \Omega_1)t)\Bigg\{-\mathrm{i}\frac{C_1(0)\sqrt{n_1}\,\sin(\gamma\sqrt{n_1 + n_2}\, t)}{\sqrt{n_1 + n_2}} \\ & + \frac{C_2(0)(n_1\cos(\gamma\sqrt{n_1 + n_2}\, t) + n_2)}{n_1 + n_2} \\ & + C_3(0)\frac{\sqrt{n_1 n_2}}{n_1 + n_2}(\cos(\gamma\sqrt{n_1 + n_2}\, t) - 1)\Bigg\}.\end{aligned} \tag{9}$$

In equations (8) and (9) we introduced the notation $\Delta_m = E_m + n_1\Omega_1 + n_2\Omega_2$. Further simplifications enabling an analytical treatment are $\langle 2|\hat{J}_z^2|1\rangle \approx \langle 3|\hat{J}_z^2|1\rangle \equiv g_0$ giving rise to the effective coupling constant $\gamma = g_0 \Delta a \delta'(a_0)$.

While the solution equations (7)–(9) is obtained for a fixed value of the magnetic field $B_0 = 4$ T, it is valid for an arbitrary field. Changing the magnetic field rescales the level spacing, thus leading to a slight rescaling of the Rabi-like transition frequencies.

The quantities we are interested in, such as level populations $I_n(t) = C_n(t)C_n^*(t)$ and von Neumann entropy $S = -\mathrm{tr}(\hat{\rho}\ln\hat{\rho})$ (where $\hat{\rho} = \sum_{mn} C_n(t)C_m^*(t)|m\rangle\langle n|$ is the density matrix of the system) can be calculated directly from (8) and (9). For this purpose we need to consider the averaging of equations (8) and (9) over the phonon distribution functions for the coherent states $w_{n_{1,2}} = \frac{\sqrt{\lambda_{1,2}^{n_{1,2}}}}{\sqrt{n_{1,2}!}}\exp\left(\frac{-\lambda_{1,2}}{2}\right)$. Here $\lambda_{1,2}$ is the mean phonon number $\lambda_{1,2} \gg 1$ corresponding to the classical limit.

For the calculations of the average level populations we perform summation over the phonon numbers n_1 and n_2:

$$\overline{I_n(t)} = \overline{|C_n(t)|^2} = \sum_{n_1,n_2=0}^{\infty} w_{n_1}^2 w_{n_2}^2 |C_n(t)|^2 = \sum_{n_1,n_2=0}^{\infty} \frac{\mathrm{e}^{-\lambda_1}\mathrm{e}^{-\lambda_2}\lambda_1^{n_1}\lambda_2^{n_2}}{n_1! n_2!}|C_n(t)|^2. \tag{10}$$

The coefficients $C_n(t)$ have a sharp maximum near the mean phonon numbers $\lambda_{1,2} \gg 1$, and the width $\Delta n_{1,2}$ of their distribution is rather small $\Delta n_{1,2} \gg \lambda_{1,2}$. This allows performing the summation analytically and obtaining expressions for the level populations and for the von Neumann entropy. The explicit expression is presented in the appendix.

With the analytical solutions at hand, we can now study the population dynamics and the von Neumann entropy of the spin system due to the interaction with the cantilever. Figure 5 depicts this dynamics with an oscillation amplitude of $\Delta a = 0.1$ Å. Due to the strong dependence of the anisotropy $\delta(a)$ on the tip-sample

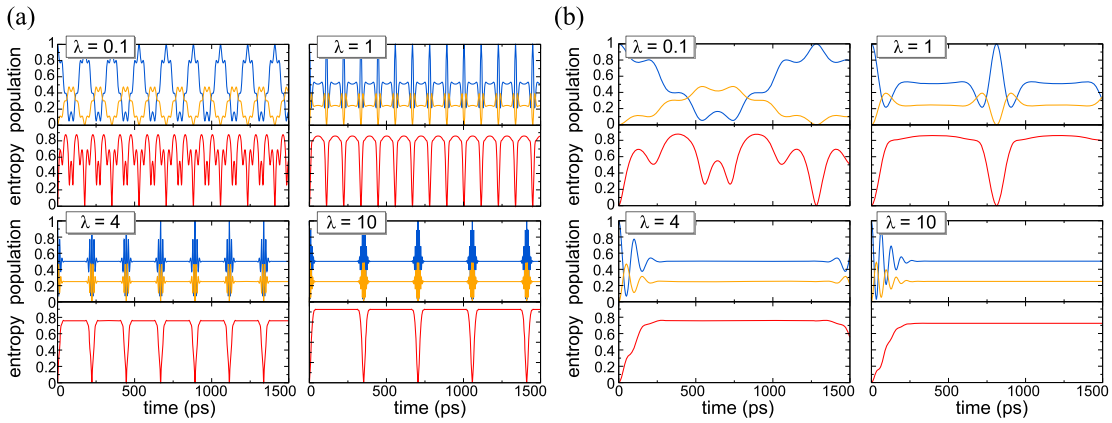

Figure 5. Population dynamics (averaged over the phonon number) of the ground state (blue) and excited state (orange) along with the von Neuman entropy for different mean photon numbers λ. In (a) the tip-sample distance is fixed at $a_0 = 3.0$ Å, while in (b) $a_0 = 4.0$ Å.

distance, the dynamics at $a_0 = 3.0$ Å (figure 5(a)) and $a_0 = 4.0$ Å (figure 5(b)) occurs on very different time scales. We clearly see that quantum revivals in level populations are synchronized with the sudden death of von Neumann entropy. This behavior is more prominent in the case of a strong coupling (figure 5(a)). Obviously with the increase of the phonon number λ the period of quantum revivals becomes larger. In the limit of the classical field $\lambda \gg 1$ the revival time tends to infinity. Meaning that the classical field like thermal bath thermalizes the system and leads to irreversibility.

6. Conclusions

In summary, we performed *ab initio* calculations of the magnetic properties of a single Fe atom adsorbed on Cu(001). We demonstrated that the electronic and the magnetic properties of adatoms are strongly affected by the tip-surface distance. Based on these results we proposed a new type of NEMS consisting of a single magnetic Fe adatoms deposited on a Cu(001) substrate and analyzed its fundamental properties and possible operation scheme.

Acknowledgments

AK acknowledges the financial support by the joint program of MSU-DAAD Vladimir Vernadsky (A/12/89268) and Volnoe Delo foundation. Computational resources were provided by the Supercomputing Center of Lomonosov Moscow State University. The work was partially funded by the German Science Foundation under SFB 762.

Appendix. von Neumann entropy

Using equations (8) and (9), a straightforward derivation yields the von Neumann entropy

$$\begin{aligned} S &= -\eta_1 \ln \eta_1 - \eta_2 \ln \eta_2 - \eta_3 \ln \eta_3, \\ \lambda_1 &= \lambda_2 = \lambda,\ \beta = \gamma\sqrt{2\lambda}t,\ \alpha = \frac{\gamma t}{\sqrt{2\lambda}}, \\ \langle I_1(t)\rangle &= \frac{1}{2}(1 + \exp\left[2\lambda(\cos\alpha - 1)\right]\cos\left(\beta + 2\lambda\sin\alpha\right)); \\ \langle I_2(t)\rangle &= \langle I_3(t)\rangle \\ &= \frac{1}{4}(1 - \exp\left[2\lambda(\cos\alpha - 1)\right]\cos\left(\beta + 2\lambda\sin\alpha\right)); \\ \langle I_4(t)\rangle &= \langle I_5(t)\rangle = 0. \end{aligned} \tag{A.1}$$

Here, we used the following notation in order to obtain a compact expression:

$$
\begin{aligned}
a &= \frac{1}{2}(1 + \exp[2\lambda(\cos\alpha - 1)]\cos(\beta + 2\lambda\sin\alpha));\\
b &= \frac{\sqrt{2}}{4}\exp[2\lambda(\cos\alpha - 1)]\sin(\beta + 2\lambda\sin\alpha);\\
d &= \frac{1}{4}\left(1 - \frac{1}{4\lambda}\right)(1 + \exp[2\lambda(\cos\alpha - 1)]\cos(\beta + 2\lambda\sin\alpha));\\
\eta_1 &= \frac{1}{16\lambda}(1 - \exp[2\lambda(\cos\alpha - 1)]\cos(\beta + 2\lambda\sin\alpha));\\
\eta_2 &= \frac{1}{4}(1 + 2d + a + \sqrt{9a^2 + 32b^2 - 6a(1 + 2d) + (1 + 2d)^2});\\
\eta_3 &= \frac{1}{4}(1 + 2d + a - \sqrt{9a^2 + 32b^2 - 6a(1 + 2d) + (1 + 2d)^2}).
\end{aligned}
\tag{A.2}
$$

References

[1] Chan J, Alegre T P M, Safavi-Naeini A H, Hill J T, Krause A, Gröblacher S, Aspelmeyer M and Painter O 2011 *Nature* **478** 89–92
[2] Ludwig M, Hammerer K and Marquardt F 2010 *Phys. Rev.* A **82** 012333
[3] Heinrich G and Marquardt F 2011 *Europhys. Lett.* **93** 18003
[4] Hammerer K, Wallquist M, Genes C, Ludwig M, Marquardt F, Treutlein P, Zoller P, Ye J and Kimble H J 2009 *Phys. Rev. Lett.* **103** 063005
[5] Rugar D, Budakian R, Mamin H J and Chui B W 2004 *Nature* **430** 329–32
[6] Arcizet O, Jacques V, Siria A, Poncharal P, Vincent P and Seidelin S 2011 *Nat. Phys.* **7** 879–83
[7] Rabl P, Cappellaro P, Dutt M V G, Jiang L, Maze J R and Lukin M D 2009 *Phys. Rev.* B **79** 041302
[8] Treutlein P 2012 *Nature* **335** 1584–5
[9] Mishra S K, Chotorlishvili L, Rau A R P and Berakdar J 2014 *Phys. Rev.* A **90** 033817
[10] Jelezko F, Gaebel T, Popa I, Gruber A and Wrachtrup J 2004 *Phys. Rev. Lett.* **92** 076401
[11] Fuchs G D, Dobrovitski V V, Toyli D M, Heremans F J and Awschalom D D 2009 *Science* **326** 1520–2
[12] Chotorlishvili L, Sander D, Sukhov A, Dugaev V, Vieira V R, Komnik A and Berakdar J 2013 *Phys. Rev.* B **88** 085201
[13] Karabalin R B, Cross M C and Roukes M L 2009 *Phys. Rev.* B **79** 165309
[14] Chotorlishvili L, Ugulava A, Mchedlishvili G, Komnik A, Wimberger S and Berakdar J 2011 *J. Phys. B: At. Mol. Opt. Phys.* **44** 215402
[15] Lifshitz R and Cross M C 2003 *Phys. Rev.* B **67** 134302–13
[16] Bromberg Y, Cross M C and Lifshitz R 2006 *Phys. Rev.* E **73** 016214
[17] Loth S, Etzkorn M, Lutz C P, Eigler D M and Heinrich A J 2010 *Science* **329** 1628–30
[18] Loth S, Baumann S, Lutz C P, Eigler D M and Heinrich A J 2012 *Science* **335** 196–9
[19] Schwöbel J, Fu Y, Brede J, Dilullo A, Hoffmann G, Klyatskaya S, Ruben M and Wiesendanger R 2012 *Nat. Commun.* **3** 953
[20] Etzkorn M *et al* 2015 *Phys. Rev.* B **92** 184406
[21] Wolter B, Yoshida Y, Kubetzka A, Hla S W, von Bergmann K and Wiesendanger R 2012 *Phys. Rev. Lett.* **109** 116102 –6
[22] Hirjibehedin C F, Lin C Y, Otte A F, Ternes M, Lutz C P, Jones B A and Heinrich A J 2007 *Science* **317** 1199–203
[23] Agarwal A K G S 2011 *Math. Comput. Appl.* **16** 290–300
[24] Blöchl P E 1994 *Phys. Rev.* B **50** 17953–79
[25] Kresse G and Joubert D 1999 *Phys. Rev.* B **59** 1758–75
[26] Kresse G and Hafner J 1993 *Phys. Rev.* B **48** 13115–8
[27] Wang Y and Perdew J P 1991 *Phys. Rev.* B **44** 13298–307
[28] Perdew J P and Wang Y 1992 *Phys. Rev.* B **45** 13244–9
[29] Błoński P, Lehnert A, Dennler S, Rusponi S, Etzkorn M, Moulas G, Bencok P, Gambardella P, Brune H and Hafner J 2010 *Phys. Rev.* B **81** 104426
[30] Kolesnikov S, Klavsyuk A and Saletsky A 2013 *Surf. Sci.* **612** 48–56
[31] Klavsyuk A L, Kolesnikov S V and Saletsky A M 2014 *JETP Lett.* **99** 646–9
[32] Hofer W A, Foster A S and Shluger A L 2003 *Rev. Mod. Phys.* **75** 1287–331
[33] Kürpick U and Rahman T S 1999 *Phys. Rev. Lett.* **83** 2765–8
[34] Huang R Z, Stepanyuk V S, Klavsyuk A L, Hergert W, Bruno P and Kirschner J 2006 *Phys. Rev.* B **73** 153404
[35] Monkhorst H J and Pack J D 1976 *Phys. Rev.* B **13** 5188–92
[36] Błoński P and Hafner J 2009 *J. Phys.: Condens. Matter* **21** 426001
[37] Stepanyuk V S, Baranov A N, Hergert W and Bruno P 2003 *Phys. Rev.* B **68** 205422
[38] Pick I C V, Stepanyuk V S, Baranov A N, Hergert W and Bruno P 2003 *Phys. Rev.* B **68** 104410
[39] Pick I C V, Stepanyuk V S, Klavsyuk A L, Niebergall L, Hergert W, Kirschner J and Bruno P 2004 *Phys. Rev.* B **70** 224419
[40] Balashov T *et al* 2009 *Phys. Rev. Lett.* **102** 257203
[41] Lazarovits B, Szunyogh L, Weinberger P and Újfalussy B 2003 *Phys. Rev.* B **68** 024433
[42] Chawla G and Solares S D 2009 *Meas. Sci. Technol.* **20** 015501
[43] Solares S D and Chawla G 2008 *Meas. Sci. Technol.* **19** 055502